DOI 10.1007/s10891-019-02015-4
Journal of Engineering Physics and Thermophysics, Vol. 92, No. 4, July, 2019

NANOSTRUCTURES

SYNTHESIS OF REINFORCED CERAMIC MATRIX COMPOSITE BASED ON SiC AND NANOCARBON MESH

D. V. Solovei,[a] P. S. Grinchuk,[a] H. M. Abuhimd,[b] M. S. Alshahrani,[b] M. V. Kiyashko,[a] M. O. Stepkin,[a] A. V. Akulich,[a] and A. A. Khort[a]

UDC 66.092-977; 543.424.2

Most modern matrix composite materials employ a variety of carbon nanofillers to improve their mechanical, electrical, and functional properties. Nanofillers are separately implanted into the initial ceramic matrix, which complicates the composite manufacturing technology and increases the final cost. In this work, the synthesis of nanocarbon fillers was carried out using high-temperature (1200°C) pyrolysis of phenolic resin directly inside the silicon carbide matrix. This results in the formation of a continuous 3D nanocarbon mesh uniformly binding and reinforcing the final product throughout the volume. The nanocarbon filler synthesized in the SiC matrix contains two allotropic carbon forms: nanographite and nanofibers. The study of the features of the carbon structure and morphology showed that during the pyrolysis the multilayered nanographite structures had been formed on the surface of SiC grains of average crystallite size equal to 20–35 nm. In the matrix pores, carbon nanofibers a few micrometers in length and 20–40 nanometers in diameter are synthesized. The reiteration of the phenolic resin impregnation–pyrolysis cycle increased the free carbon content from 4 to 7 wt.% for once and twice impregnated and pyrolyzed samples, respectively, and the Young's modulus, from 50.7 to 94.3 GPa. The obtained carbon content and structure are appropriate to produce C/SiC composite for application of ceramics and electrodes.

Keywords: *SiC, nanographite, carbon nanofibers, ceramic matrix composite.*

Introduction. Interest in silicon carbide, which is known to be one of the most widely used oxygen-free ceramic materials, constantly increases over the last decades. This is due to a number of unique physical, chemical, and mechanical properties allowing the use of SiC for airspace application, in nuclear power stations, for armor production, in radioelectronic industry, etc. Silicon carbide is a promising material for manufacturing light, strong, as well as thermally and chemically resistant products. It is also widely used for production of semiconductor substrates, tools, and optical elements. Such a variety of possible application areas is due to its crystal structure, which results from the nature of carbon and silicon atoms, as well as strong covalent bonds between them [1–10].

However, despite many advantages of silicon carbide-based ceramics, the manufacturing process is labor-intense and time-consuming; in addition, this ceramic features low fracture toughness and high brittleness [11–14]. As an alternative to silicon carbide ceramics, ceramic composite materials have been developed; these materials are less brittle and have higher fracture toughness, as well as a lower density [15–19]. Such materials employ silicon carbide as a matrix but include reinforcing additives usually based on various allotropic carbon forms: nanofibers, whiskers, nanotubes, graphene, graphene oxide, graphene nanoflakes and nanoplatelets [20–26]. Unfortunately, these additives have a limited size and length and cannot create a continuous and uniform grid in the form of a mesh that would reinforce the original 3D silicon carbide matrix throughout the whole volume. This requires the availability of high-tech cost-expensive equipment, which imposes limitations on the size of the produced product in spark plasma sintering (SPS), hot isostatic pressing (HIP), and high-frequency induction heated sintering (HFIHS) [27–29].

[a]A. V. Luikov Heat and Mass Transfer Institute, National Academy of Sciences of Belarus, 15 P. Brovka Str., Minsk, 220072, Belarus; email: solovei@hmti.ac.by; [b]National Nanotechnology Research Center, King Abdulaziz City for Science and Technology, Riyadh, 11442, P.O. Box 6086, Saudi Arabia. Published in Inzhenerno-Fizicheskii Zhurnal, Vol. 92, No. 4, pp. 1050–1058, July–August, 2019. Original article submitted January 29, 2019.

Several methods for implantation of carbon nanofillers into a ceramic matrix composite material have been developed: the use of powders and colloidal solutions, sol-gel processes, and implantation of nanocarbon into a polymer and its subsequent additiont to the composite. After the formation of ceramic and carbon parts of the composite and their thorough mixing, a sintering process is carried out at a high temperature. Sintering can be performed via either a traditional route or a novel one, such as hot pressing, HIP, SPS, HFIHS, and microwave heating [27–31]. The aforesaid methods imply the addition of a nanocarbon material, which is produced separately and is available on the market. Thus, the purchase of nanocarbon, its preparation (milling, dispersing, forming sol-gels, etc.), and the creation of a mixture of ceramics and nanocarbon and subsequent sintering are time-consuming and expensive processes for the production of a ceramic composite material.

In this paper, a low-cost and technologically feasible method for the fabrication of a ceramic composite material for products with linear dimensions of several tens of centimeters is described; the proposed method can be easily adapted to much larger sizes. The purpose of this work is the formation of a reinforced ceramic matrix composite based on silicon carbide with a continuous nanocarbon mesh throughout the volume with the possibility of controlling the percentage of a nanocarbon filler in the final product, as well as studying the morphological, microstructural, and mechanical features of the resulting composite by scanning electron microscopy (SEM), micro-Raman analysis, and mechanical tests.

Experimental. All experimental samples (discs 200 mm in diameter and 14 mm in thickness) were obtained by powder injection molding (PIM) from a slip mass at 85^{o}C under the pressure 0.5 MPa. The slip mass was obtained by mixing 87.5 wt.% of green silicon carbide powders (62.5 wt.% of M50 SiC powder and 37.5 wt.% of M5 SiC powder, both from Volzhsky Abrasive Works, Russia) with 12.5 wt.% of a thermoplastic paraffin-based binder. The binder was removed from the green body by heating at 600^{o}C for 2 h in a kaolin backfill in the air atmosphere. After cooling and cleaning from kaolin, the green body was impregnated with phenolic resin (Bakelite lacquer of LBS-1 brand from Ya. M. Sverdlov Plant, Russia). To carry out impregnation, the green sample was placed into an evacuated tank and then resin was fed into it. The impregnation process was described in detail in [32]. After that, nitrogen was pumped into the tank at a pressure of 0.35 MPa. Impregnation was carried out for 5 h. Under such conditions, all open pores were uniformly filled with phenolic resin, which was confirmed by measuring the mass of the green samples before and after impregnation, taking into account the resin density. After drying in air for 30 min, the green specimen was placed into a drying oven where it was slowly heated up to 120^{o}C. This is necessary for complete removal of water and alcohol contained in phenolic resin. After that, the green body was placed in a vacuum furnace where pyrolysis was carried out at 1200^{o}C and pressure 10^{-1} Pa for 2 h. For analysis, the samples were cut out using a laboratory cutting machine with a diamond cutting disk (Metacut 251), carefully washed in distilled water, and dried. The samples of two types were prepared by using the above-described method: No. 1 is a once impregnated and pyrolyzed sample, and No. 2 is the sample for which the impregnation–pyrolysis cycle was performed twice.

The grain size of the initial powders was measured by dispersing them in distilled water under normal conditions, using a Mastersizer 3000 particle analyzer. The density of the samples was measured by the Archimedes method in distilled water using Ohaus PA214C analytical scales. Before measuring the density, the samples were carefully washed in an ultrasonic bath filled with distilled water for complete removal of air bubbles from the micropores.

The specimen morphology and microstructure were studied using a Leo-1420 scanning electron microscope at the accelerating voltage 20 kV. Micro-Raman spectra were obtained at room temperature, using a Nanofinder High End confocal spectrometer (LOTIS TII, Belarus–Japan). A solid-state laser (532 nm, 20 mW) was used to excite the signal. Laser radiation was focused on the specimen surface by a 50× lens with a numerical aperture of 0.8. In this case, the excitation region was of the order of 1 μm in diameter. The power of laser radiation was attenuated to 2 mW to avoid thermal damage to the sample. The back-scattered light was dispersed by a 600 mm^{-1} diffraction grating, which provided a spectral resolution of at least 3 cm^{-1}. A polarizer in a registration channel was not installed. Preliminary spectral calibration along the lines of a gas-discharge lamp ensured an accuracy of at least 3 cm^{-1}. The accumulation time of the signal was 30 s. A deep-cooled silicon CCD-matrix was used as a photodetector.

The indentation tests were performed using a Hysitron TI750 Ubi with a Berkovich tip to determine the Young′s modulus of the C/SiC composite.

Results and Discussion. Figure 1 displays photographs of the experimental samples after the main technological stages: slip casting of the preform and removal of an organic binder (Fig. 1a) and impregnation with phenolic resin and pyrolysis (Fig. 1b). After the removal of the organic binder, the porosity of the silicon carbide matrix was 33%, while the preform had sufficient mechanical strength for subsequent processing operations. With subsequent impregnation and pyrolysis, the resulting composite material acquired a uniform black color associated with the formation of a pyrolyzed carbon residue throughout the product volume, as seen in the corresponding cross section (Fig. 1b).

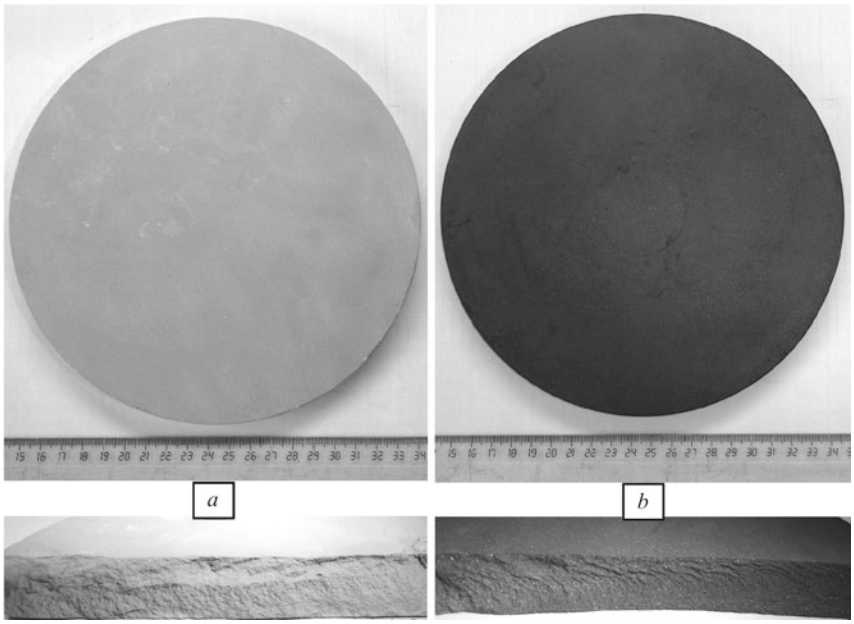

Fig. 1. Top view and cross section of: the SiC preform after removal of the organic binder (a) and the ceramic matrix composite "SiC/nanocarbon" (b).

Figure 2 shows the SEM images and Raman spectra of the raw M50 and M5 powders. As can be seen in the SEM images (Fig. 2a and b), the initial commercial silicon carbide powders consist of complex-shape grains with clearly seen cleavage surfaces resulting from brittle fracture. Figure 2c and d shows the Raman spectra of the initial SiC powders of two fractions used: M50 (99% SiC) and M5 (97% SiC). There are two clearly expressed peaks at about 787 and 968 cm^{-1} that belong to vibrations of the covalent bond (Si–C) of crystalline silicon carbide. The 787 cm^{-1} peak refers to transversal optical phonon vibrations of E_1 (TO) symmetry, and the peak located in the region of 968 cm^{-1}, to longitudinal optical phonon vibrations of A_1 (LO) symmetry in the SiC crystal structure. Moreover, the 787 cm^{-1} peak is doubled with the second maximum at 765 cm^{-1} which belongs to transversal optical phonon vibrations of E_2 (TO) symmetry. In addition, there is a weak vibration peak at about 505 cm^{-1} and a peak of the second order at about 1515 cm^{-1} in the spectra. Thus, basing on the Raman spectroscopy, we conclude that the initial SiC powders belong to one of the most common hexagonal 6H–SiC polytype [33–35]. No free-carbon structures were detected on the surface of the SiC grains.

The temperature for carbonization of phenolic resin was chosen according to the data presented in [36–40]. During carbonization, the maximum weight loss of resin was detected in the temperature range from 300 to 600^{o}C, and this process was almost completed at about 800^{o}C. Nevertheless, in the range 800–1100^{o}C, the weight loss increased by 2%, and the density of the carbonized residual increased from 1.3 to about 1.5 g/cm^3. At the temperature 1200^{o}C, small graphitic packets are observed inside the glass-like structure of carbon generated by pyrolysis of phenolic resin at lower temperatures. These packets grow with time both in number and in size [39, 40]. Basing on this information, the temperature 1200^{o}C was chosen for the carbonization process.

Figure 3 shows the SEM images of inner morphology of the samples of both types: a once impregnated and pyrolyzed sample (No. 1) and a twice impregnated and pyrolyzed sample (No. 2). It can be clearly seen that the microstructure of the samples presents a bimodal mixture of coarse and fine SiC particles (cf. Fig. 1) bound together by thin layers of pyrolytic carbon derived from phenolic resin. Some silicon carbide grains were knocked out, and a complex relief appeared during cutting. Sample No. 2 is characterized by a denser structure with fewer pores than sample No. 1 due to the higher amount of carbon in the pores and on the surface of SiC particles. As seen in the SEM images, carbon covers the grains of silicon carbide with one or more layers, with a single layer thickness of about 40 nm (separate carbon layers are marked with arrows in Fig. 3b). Carbon layers contain a large number of structural defects and ruptures at edges and at points of contact with SiC grains. In addition, there are carbon nanofibers of several micrometers (limited by the pore size) in length and tens of nanometers (20–40 nm) in diameter that are present in the SEM images. Nanofibers are synthesized in the matrix pores,

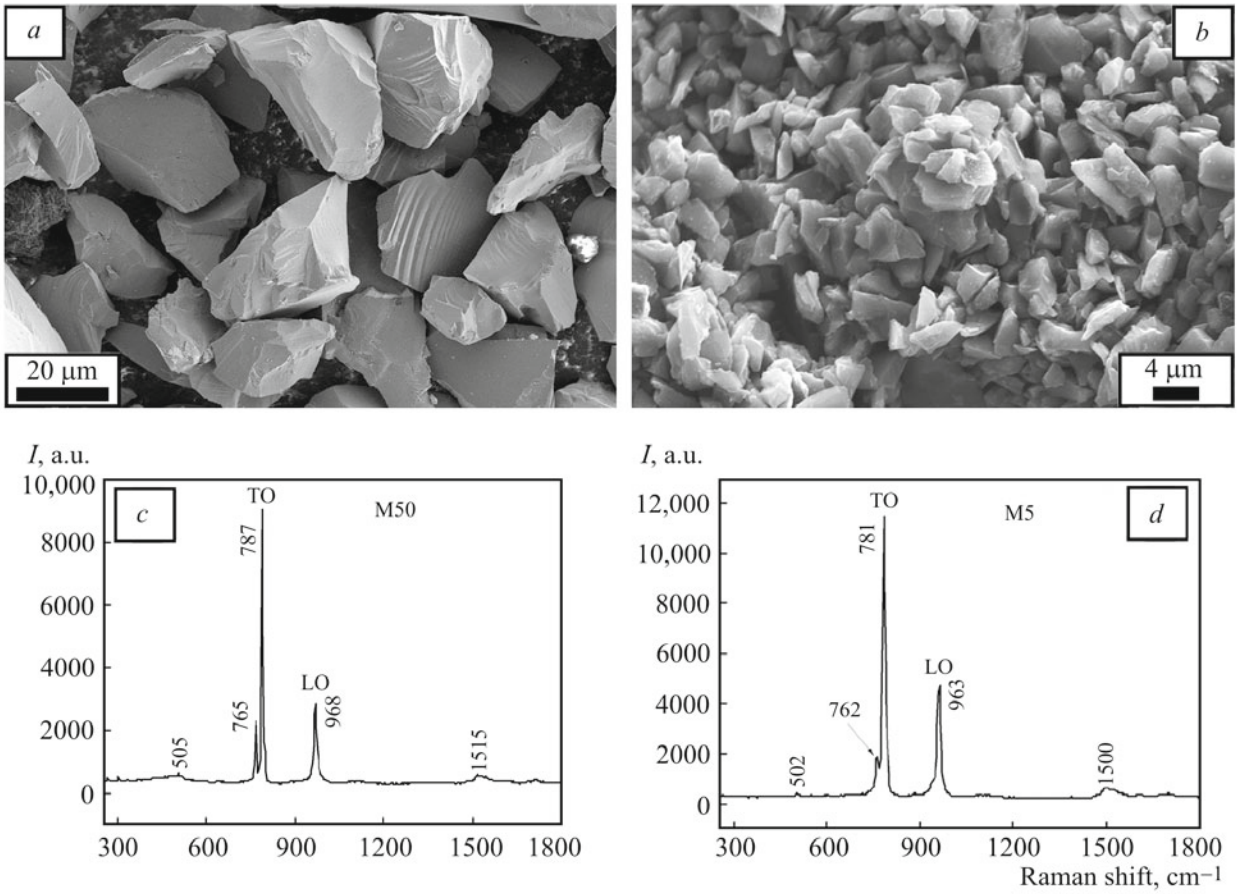

Fig. 2. SEM images and Raman spectra of initial SiC powders: large fraction of silicon carbide M50 of average grain size equal to 54 μm (a and c); small fraction of silicon carbide M5 of average grain size equal to 4 μm (b and d).

probably forming the bridges between SiC grains. In general, the morphology of the carbon layers is determined to a large extent by the inner structure of the initial silicon carbide matrix that was formed during the sample preparation.

According to the SEM images, the number of the visible pores in sample No. 1 is higher than that in sample No. 2. The higher porosity of sample No. 1 was confirmed by the results of density measurements for both samples. The measured density of sample No. 1 was 2.35 g/cm^3, whereas that of sample No. 2 reached 2.43 g/cm^3, which points to a higher amount of carbon. Thus, after the first impregnation and pyrolysis cycle, each sample collected about 4 wt.% of carbon, and after the second cycle the carbon content increased to 7 wt.% of the initial sample mass (i.e., the second cycle gained additional 3 wt.% of carbon by filling residual open-pore space).

The Raman spectra of the experimental samples shown in Fig. 4 permitted detecting two allotropic forms of carbon: nanographite (NG) and carbon nanofibers (CNF). These carbon forms are present in the spectra of both types of the samples: the blue curve is the spectrum of nanographite, and the black one refers to the spectrum of nanofibers.

Raman spectra of nanographite (blue curve). As can be seen, the spectra of both types of the samples are characterized by the same crystal structure and positions of the major carbon peaks. The main difference consists of the peak intensity and small deviations from the maxima. The same three peaks of carbon are clearly seen in the spectra of both sample types (Nos. 1 and 2): G peak (1582 and 1586 cm^{-1} for samples Nos. 1 and 2, respectively), D peak (1347 and 1345 cm^{-1} for samples Nos. 1 and 2), and G′ peak (2693 cm^{-1} for both sample types). In addition, the D′ defective shoulder with a frequency of 1617 cm^{-1} was found in the G peak of both sample types. The main peak of the second-order region G′ is the overtone of the D peak. The extra peak G_1' (2448 and 2452 cm^{-1} for samples Nos. 1 and 2) was assigned to the band as the "$q = 0$" branch of the double resonance Raman scattering, and the extra peak G_2' (2931 and 2933 cm^{-1} for samples Nos. 1 and 2) appeared as a sum of the D and G peaks [41–44]. The presence of both peaks of the first and second orders in the Raman spectra indicates

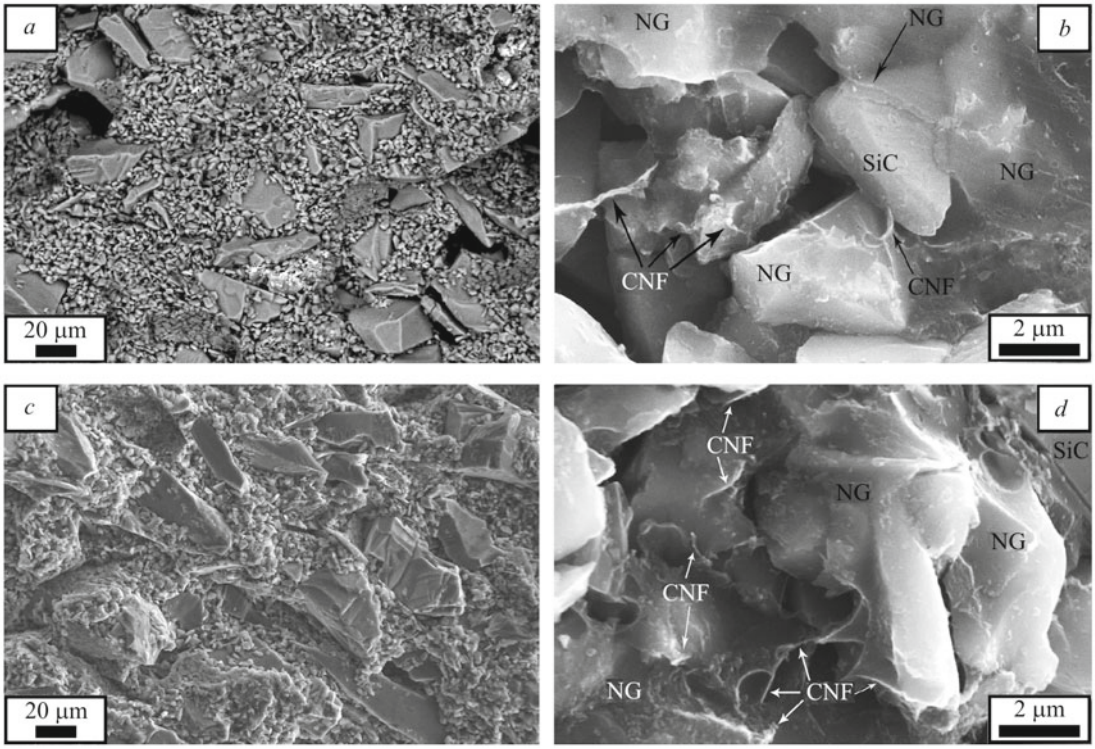

Fig. 3. Microstructure SEM images of silicon carbide samples reinforced with nanocarbon mesh after pyrolysis at 1200°C: a and b) one impregnation–pyrolysis process (sample No. 1); c and d) two impregnation–pyrolysis processes (sample No. 2). Nanographite layers (NG) and carbon nanofibers (CNF) are marked with arrows.

that pyrolytic carbon includes disordered polycrystalline nanographite with C–C sp^2-type hybridization bonds. It is related to vibrations of the E_{2g} type structure and corresponds to the displacement of carbon atoms in the base plane. The Raman spectra contain also peaks that belong to silicon carbide. The values of their maxima correspond to those of the initial raw SiC powders (Fig. 2). By this is meant that no significant structural changes in SiC powders were observed during pyrolysis at 1200°C.

The size of a single crystallite of nanographite L_a was calculated according to [41, 45] from the following equation:

$$L_a = 2.4 \cdot 10^{-10} \lambda^4 \left(\frac{I_D}{I_G} \right)^{-1} .$$

The calculated crystallite sizes of carbonized resin in samples Nos. 1 and 2 are 20 and 34 nm, respectively. We suppose that the difference in the sizes of crystallites is due to the higher content of carbon in sample No. 2. The latter is due to the fact that carbon was introduced into the silicon carbide matrix by two impregnation cycles with additional heat treatment at 1200°C, which activated the carbon grain growth. We also believe that an increase in the size of crystallites and in the total content of nanocarbon in the final composite material will lead to an increase in its functional characteristics.

Raman spectra of carbon nanofibers (black curve). The spectrum of carbon nanofibers is similar to that presented in [5, 46, 47]. Compared to the nanografite spectrum, it has a significantly lower intensity of three main peaks located in the same D, G, and G′ regions: 1344, 1586, and 2693 cm^{-1} for sample type No. 1 and 1328, 1566, and 2681 cm^{-1} for sample type No. 2, while the peak G′ does not have pronounced side peaks G'_1 and G'_2. The main difference between the spectra of two carbon forms (nanographite and nanofibers) is the ratio of the maximal intensities I_D/I_G. For nanofibers, this ratio is 1.13 for sample No. 1 and 0.94 for sample No. 2, while for nanographite this ratio is 0.91 and 0.57 for these samples. For nanofibers this ratio is close to unity, and for nanographite it approaches 0.5 as the number of impregnation and pyrolysis cycles increases. The second difference in the spectra of nanographite and nanofibers is that the SiC reflex is strongly pronounced in

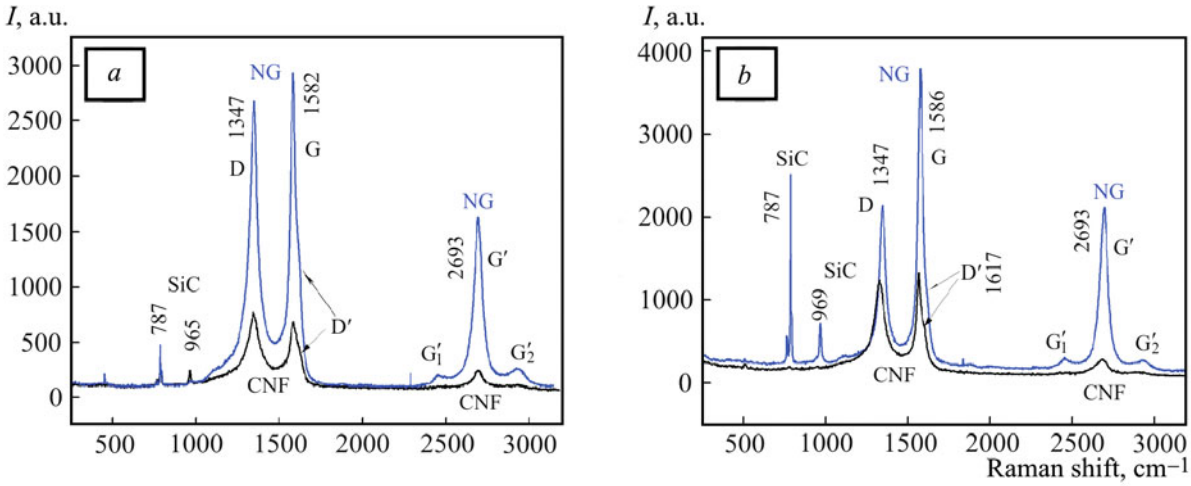

Fig. 4. Raman spectra of SiC-based samples reinforced with nanocarbon mesh produced by pyrolysis at 1200°C, including nanographite NG (blue curve) and carbon nanofibers CNF (black curve): a) one impregnation–pyrolysis process (sample No. 1); b) two impregnation–pyrolysis processes (sample No. 2).

the spectra of nanographite, especially for sample No. 2 (blue curve), and for nanofibers it either does not exist (Fig. 3b) or is very small (Fig. 3a). This may be ascribed to the fact that nanofibers are formed in the pore space and contact with the grains of silicon carbide by their tips. The nanographite layers are formed directly on the surface of the SiC grains and are located over a large area in the immediate connection with them.

We suppose that the conditions of pyrolysis of phenolic resin, as well as the initial structure and morphology of SiC matrix, determine the structure of different carbon types. They are formed during pyrolysis and are accompanied by the formation of various structural defects.

The measured value of the Young′s modulus of the reinforced ceramic matrix composite based on SiC nanocarbon mesh for one phenolic resin impregnation–pyrolysis cycle is 50.7 GPa, and for twice impregnated and pyrolyzed samples is 94.3 GPa. The obtained values are typical of carbon/composite materials [48–51].

Thus, the use of phenolic resin and high-temperature pyrolysis make it possible to obtain a 3D composite material containing a nanocarbon mesh whose microstructure consists of nanographite and carbon nanofibers uniformly covering, binding, and reinforcing the grains of the original SiC matrix. Further research will be aimed at determining the thermal and electrophysical properties of the resulting composite, as well as at its application for the production of dense silicon carbide ceramics [52] and electrodes for energy storage devices.

Conclusions. A ceramic matrix composite based on silicon carbide and nanocarbon was produced using low-pressure slip casting and impregnation with phenolic polymer resin followed by high-temperature pyrolysis. Nanocarbon, which forms a 3D mesh that uniformly covers the silicon carbide grains throughout the whole volume of the composite, thus providing strong bonding of the grains to each other, contains two allotropic forms: nanographite and carbon nanofibers. Nanographite appears in close contact with the silicon carbide grains, while nanofibers are located predominantly in the pores of the original matrix. With the use of the micro-Raman analysis, nanographite layers were revealed in the obtained carbon that are characterized as a polycrystalline structure with a crystallite size of several tens of nanometers. The length of carbon nanofibers in the composite is several micrometers, which is comparable with the pore size, and the diameter is about 20–40 nm. The structure and morphology of the pyrolyzed residue are determined by the arrangement and packaging of the silicon carbide grains formed during casting of the green body by the PIM method. It is found that reiteration of the impregnation–pyrolysis cycles has increased the content of carbon inside of SiC matrix from 4 to 7 wt.% and the Young′s modulus from 50.7 to 94.3 GPa.

As a result, the developed technology allows obtaining bulk products consisting of a ceramic matrix composite material with a controlled carbon content, which is supposed to improve the strength and performance characteristics. The properties of the material will be a subject of further studies.

Acknowledgments. This work was supported by the King Abdulaziz City for Science and Technology (Saudi Arabia).

The authors are grateful to Dr. Mikhail Tivanov (Belorussian State University) for micro-Raman analysis of the materials and to Prof. Boris Khina (Physicotechnical Institute, National Academy of Sciences of Belarus) for improving the English text.

NOTATION

I_D and I_G, intensities of D and G spectral peaks, respectively, a.u.; L_a, size of a single crystallite of nanographite, nm; λ, wavelength of laser radiation, nm.

REFERENCES

1. N. P. Bansal, *Handbook of Ceramic Composites*, Kluwer Academic Publishers, Boston (2005).
2. E. A. Belyaeva and R. V. Konakova, *Silicon Carbide: Technology, Properties, Application* [in Russian], Scintillation Materials Inst., Khar′kov (2010).
3. L. Borchardt, C. Hoffmann, M. Oschatz, L. Mammitzsch, U. Petasch, M. Herrmann, and S. Kaskel, Preparation and application of cellular and nanoporous carbides, *Chem. Soc. Rev*., **15**, No. 41, 5053–5067 (2012).
4. F. Jiang, Y. Liu, Y. Yang, Z.-R. Huang, D. Li, G.-L. Liu, and X.-J. Liu, Research progress of optical fabrication and surface-microstructure modification of SiC, *J. Nanomater.*, **2012**, ID 984048, 9 pp. (2012).
5. J. H. Eom, Y. W. Kim, and S. Raju, Processing and properties of macroporous silicon carbide ceramics. A review, *J. Asian Ceram. Soc*., **1**, No. 3, 220–242 (2013).
6. N. P. Bansal and J. Lamon, *Ceramic Matrix Composites*: *Materials, Modeling and Technology,* John Wiley & Sons Inc., Hoboken, New Jersey (2015).
7. W. Krenkel, B. Heidenreich, and R. Renz, C/C–SiC composites for advanced friction systems, *Adv. Eng. Mater*., **4**, No. 7, 427–436 (2002).
8. A. Ortona, D. Trimis, V. Uhlig, R. Eder, S. Gianella, P. Fino, G. D'Amico, E. Boulet, C. Chazelas, T. Gramer, E. Cresci, J. G. Wunning, H. Altena, F. Beneke, and M. Debier, Si–SiC heat exchangers for recuperative gas burners with highly structured surface elements, *Int. J. Appl. Ceram. Technol*., **11**, No. 5, 927–937 (2014).
9. M. Li, X. Zhou, H. Yang, S. Du, and Q. Huang, The critical issues of SiC materials for future nuclear systems, *Scr. Mater.*, **143**, 149–153 (2018).
10. W. J. Kim, D. Kim, and J. Y. Park, Fabrication and material issues for the application of SiC composites to LWR fuel cladding, *Nucl. Eng. Technol.*, **45**, No. 4, 565–572 (2013).
11. M. Belmonte, P. Miranzo, and M. I. Osendi, Contact damage resistant SiC/graphene nanofiller composites, *J. Eur. Ceram. Soc.*, **38**, No. 1, 41–45 (2018).
12. G. Choubey, L. Suneetha, and K. M. Pandey, Composite materials used in Scramjet — A review, *Mater. Today: Proc*., **5**, No. 1, 1321–1326 (2018).
13. Y. Xie, L. Cheng, L. Li, H. Mei, and L. Zhang, Fabrication of laminated SiCw/SiC ceramic composites by CVI, *J. Eur. Ceram. Soc*., **33**, No. 10, 1701–1706 (2013).
14. R. Sedlak, A. Kovalcikova, V. Girman, E. Mudra, P. Rutkowski, A. Dubiel, and J. Dusza, Fracture characteristics of SiC/graphene platelet composites, *J. Eur. Ceram. Soc*., **37**, No. 14, 4307–4314 (2017).
15. H. Wangn, D. Zhu, Y. Mu, W. Zhou, and F. Luo, Effect of SiC/C preform densities on the mechanicaland electromagnetic interference shielding properties of dual matrix SiC/C–SiC composites, *Ceram. Int*., **41**, No. 10, 14094–14100 (2015).
16. K. P. Tonello, E. Padovano, C. Badini, S. Biamino, M. Pavese, and P. Fino, Fabrication and characterization of laminated SiC composites reinforced with graphene nanoplatelets, *Mater. Sci. Eng. A*, **659**, 158–164 (2016).
17. P. Miranzo, M. Belmonte, and M. I. Osendi, From bulk to cellular structures: A review on ceramic/graphene filler composites, *J. Eur. Ceram. Soc*., **37**, No. 12, 3649–3672 (2017).
18. K. Kollins, C. Przybyla, and M. S. Amer, Residual stress measurements in melt infiltrated SiC/SiC ceramic matrix composites using Raman spectroscopy, *J. Eur. Ceram. Soc*., **38**, No. 7, 2784–2791 (2018).
19. J. Yina, S. H. Lee, L. Feng, Y. Zhu, X. Liu, Z. Huang, S. Y. Kim, and I. S. Han, The effects of SiC precursors on the microstructures and mechanical properties of SiCf/SiC composites prepared via polymer impregnation and pyrolysis process, *Ceram. Int*., **41**, No. 3, 4145–4153 (2015).

20. O. Hanzel, R. Sedlak, J. Sedlaceka, V. Bizovska, R. Bystricky, V. Girman, A. Kovalcikova, J. Dusza, and P. Sajgalik, Anisotropy of functional properties of SiC composites with GNPs, GO and *in-situ* formed graphene, *J. Eur. Ceram. Soc*., **37**, No. 12, 3731–3739 (2017).
21. R. Cano-Crespo, B. M. Moshtaghioun, D. Gomez-Garcia, A. Domínguez-Rodríguez, and R. Moreno, Carbon nanofibers replacing graphene oxide in ceramic composites as a reinforcing phase: Is it feasible? *J. Eur. Ceram. Soc*., **37**, No. 12, 3791–3796 (2017).
22. S. Tang and C. Hu, Design, preparation and properties of carbon fibers reinforced ultrahigh temperature ceramic composites for aerospace applications: A review, *J. Mater. Sci. Technol.,* **33**, No. 2, 117–130 (2017).
23. Y. Lu, Y. Wang, H. Shen, Z. Pan, Z. Huang, and L. Wu, Effects of temperature and duration on oxidation of ceramic composites with silicon carbide matrix and carbon nanoparticles, *Mater. Sci. Eng. A*, **590**, 368–373 (2014).
24. N. Song, H. Liu, and J. Z. Fang, Fabrication and mechanical properties of multi-walled carbon nanotube reinforced reaction bonded silicon carbide composites, *Ceram. Int*., **42**, No. 1A, 351–356 (2016).
25. C. Jimenez, K. Mergia, M. Lagos, P. Yialouris, I. Agote, V. Liedtke, S. Messoloras, Y. Panayiotatos, E. Padovano, C. Badini, C. Wilhelmi, and J. Barcena, Joining of ceramic matrix composites to high temperature ceramics for thermal protection systems, *J. Eur. Ceram. Soc*., **36**, No. 3, 443–449 (2016).
26. M. Petrus, J. Woźniak, T. Cygan, B. Adamczyk-Cieślak, M. Kostecki, and A. Olszyna, Sintering behaviour of silicon carbide matrix composites reinforced with multilayer graphene, *Ceram. Int*., **43**, No. 6, 5007–5013 (2017).
27. A. Nieto, A. Bisht, D. Lahiri, C. Zhang, and A. Agarwal, Graphene reinforced metal and ceramic matrix composites: A review, *Int. Mater. Rev.*, **62**, No. 5, 241–302 (2017).
28. H. Porwal, S. Grasso, and M. J. Reece, Review of graphene–ceramic matrix composites, *Adv. Appl. Ceram*., **112**, No. 8, 443–454 (2013).
29. K. Markandan, J. K. Chin, and M. T. T. Tan, Recent progress in graphene based ceramic composites: A review, *J. Mater. Res.*, **32**, No. 1, 84–106 (2017).
30. J. K. Kwang, H. J. Seung, K. Young-Wook, J. Byung-Koog, and N. Toshiyuki, Conductive SiC ceramics fabricated by spark plasma sintering, *Ceram. Int.,* **42**, No. 5, 17892–17896 (2016).
31. L. Hanqin, Y. Xiumin, H. Zhengren, Z. Yuping, and S. Bizhe, Effect of sintering techniques on the microstructure of liquid-phase-sintered SiC ceramics, *J. Eur. Ceram. Soc*., **36**, No. 8, 1863–1871 (2016).
32. A. Gardziella, L. A. Pilato, and A. Knop, *Phenolic Resins. Chemistry, Applications, Standardization, Safety and Ecology*, Springer-Verlag, Berlin (2000).
33. S. Lin, Z. Chen, L. Li, and C. Yang, Effect of impurities on the Raman scattering of 6H–SiC crystals, *Mater. Res.*, **15**, No. 6, 833–836 (2012).
34. E. López-Honorato, P. J. Meadows, J. Tan, and P. Xiao, Control of stoichiometry, microstructure, and mechanical properties in SiC coatings produced by fluidized bed chemical vapor deposition, *J. Mater. Res.,* **23**, No. 6, 1785–1796 (2008).
35. S. Sorieul, X. Kerbiriou, J. M. Costantini, L. Gosmain, G. Calas, and C. Trautmann, Optical spectroscopy study of damage induced in 4H–SiC by swift heavy ion irradiation, *J. Phys.: Condens. Matter*, **24**, 125801, 7 pp. (2012).
36. C. R. Choe and K. H. Lee, Effect of processing parameters on the mechanical properties of carbonized phenolic resin, *Carbon*, **30**, No. 2, 247–249 (1992).
37. J. Wang, H. Jiang, and N. Jiang, Study on the pyrolysis of phenol–formaldehyde (PF) resin and modified PF resin, *Thermochim. Acta*, **496**, Nos. 1–2, 136–142 (2009).
38. H. W. Wong, J. Peck, R. E. Bonomi, J. Assif, F. Panerai, G. Reinisch, J. Lachaud, and N. N. Mansour, Quantitative determination of species production from phenol–formaldehyde resin pyrolysis, *Polym. Degrad. Stabil.*, **112**, 122–131 (2015).
39. Z. L. Zhang, R. Brydson, Z. Aslam, S. Reddy, A. Brown, A. Westwood, and B. Rand, Investigating the structure of non-graphitising carbons using electron energy loss spectroscopy in the transmission electron microscope, *Carbon*, **49**, No. 15, 5049–5063 (2011).
40. P. Cheng, G. J. Qiao, D. C. Li, J. Q. Gao, H. J. Wang, and Z. H. Jin, RB-SiC ceramics derived from the phenol resin added with starch, *Key Eng. Mater*., **336–338**, No. 11, 1144–1147 (2007).
41. M. A. Pimenta, G. Dresselhaus, M. S. Dresselhaus, L. G. Cancado, A. Jorio, and R. Saito, Studying disorder in graphite-based systems by Raman spectroscopy, *Phys. Chem. Chem. Phys.*, **9**, 1276–1290 (2007).
42. S. Reich and C. Thomsen, Raman spectroscopy of graphite, *Philos. Trans. Roy. Soc. Lond. A*, **362**, 2271–2288 (2004).

43. A. C. Ferrari, Raman spectroscopy of graphene and graphite: Disorder, electron–phonon coupling, doping and nonadiabatic effects, *Solid State Commun.*, **143**, Nos. 1–2, 47–57 (2007).
44. B. Zhang, Y. Xue, K. Gao, L. Qiang, Y. Yu, Z. Gong, A. Liang, J. Zhang, and B. Yang, Pencil sketch graphene films as solid lubricant on steel surface: observation of transition to graphene/amorphous carbon, *Solid State Sci.*, **75**, 71–76 (2018).
45. Y. M. Shulga, N. Y. Shulga, and Y. N. Parkhomenko, Carbon nanostructures reduced from graphite oxide as electrode materials for supercapacitors, *Mater. Electron. Eng.,* **17**, No. 3, 157–186 (2014).
46. M. Llorens-Gamez and A. Serrano-Aroca, Low-cost advanced hydrogels of calcium alginate/carbon nanofibers with enhanced water diffusion and compression properties, *Polymers*, **10**, 405, 11 pp. (2018).
47. A. Ambrosi and M. Pumera, Stacked graphene nanofibers for electrochemical oxidation of DNA bases, *Phys. Chem. Chem. Phys.*, **12**, 8943–8947 (2010).
48. S. Zhang, X. Gao, H. Dong, X. Ju, and Y. Song, *In situ* modulus and strength of carbon fibers in C/SiC composites, *Ceram. Int*., **43**, No. 9, 6885–6890 (2017).
49. P. Kumar and V. K. Srivastava, Tribological behavior of C/C–SiC composites — A review, *J. Adv. Ceram.*, **5**, No. 1, 1–12 (2016).
50. D. Han, H. Mei, S. Xiao, K. G. Dassios, and L. Cheng, A review on the processing technologies of carbon nanotube/silicon carbide composites, *J. Eur. Ceram. Soc*., **38**, No. 11, 3695–3708 (2018).
51. L. C. Pardini and M. L. Gregori, Modeling elastic and thermal properties of 2.5D carbon fiber and carbon/SiC hybrid matrix composites by homogenization method, *J. Aerospace Technol. Manage.*, **2**, No. 2, 183–194 (2010).
52. P. S. Grinchuk, M. V. Kiyashko, H. M. Abuhimd, M. S. Alshahrani, M. O. Stepkin, V. V. Toropov, A. A. Khort, D. V. Solovei, A. V. Akulich, M. D. Shashkov, and M. Y. Liakh, Effect of technological parameters on densification of reaction bonded Si/SiC ceramics, *J. Eur. Ceram. Soc*., **38**, No. 15, 4815–4823 (2018).